Ionics (2021) 27:3769–3776
https://doi.org/10.1007/s11581-021-04131-9

ORIGINAL PAPER

Preparation and electrochemical properties of Ti-doped $LiNi_{1/3}Co_{1/3}Mn_{1/3}O_2$ cathode materials via co-precipitation route

Lina Yv[1] · Jing Wang[1] · Xuetan Li[1] · Lijing Dai[1] · Zhongcai Shao[2]

Received: 6 April 2021 / Revised: 17 May 2021 / Accepted: 7 June 2021 / Published online: 9 July 2021

Abstract

$LiNi_{1/3}Co_{1/3-1/20}Mn_{1/3}Ti_{1/20}O_2$ composite was prepared by co-precipitation route. The inflect of Ti-doped on the structure, morphology, and electrochemical properties of the materials were analyzed by X-ray diffraction (XRD), scanning electron microscopy and energy dispersive spectrometer (SEM–EDS), charge and discharge battery test, electrochemical impedance spectroscopy (EIS), and cyclic voltammetry. The material with doping Ti^{4+} had a small particle size, regular shape, and high crystallinity. The initial discharge specific capacity of 0.1 C was 170.3 $mAh{\cdot}g^{-1}$ with a coulombic efficiency of 98%. After 30 cycles, the specific discharge capacity was 162.3 $mAh{\cdot}g^{-1}$, and the capacity retention rate was 95%. Doping Ti^{4+} is beneficial to improve the cycle and rate performance of $LiNi_{1/3}Co_{1/3}Mn_{1/3}O_2$ material.

Keywords Doping modification · Cathode material · Electrochemical performance · Lithium-ion battery

Introduction

Lithium-ion battery is ranked as one of the best sources of energy [1]. Compared with the traditional batteries, the lithium-ion battery has the advantages of light weight, high energy density, high temperature, long service life, low self-discharge rate, high safety performance, and green economy [2, 3].

$LiNi_{1/3}Co_{1/3}Mn_{1/3}O_2$ cathode material which was initially reported by Yabuuchi and Ohzuku [4] has attracted the attention of relevant researchers. Deng et al. [5] investigated the crystal and electronic structures of $LiCo_{1/3}Ni_{1/3}Mn_{1/3}O_2$ using first principles calculations; the result showed that $LiCo_{1/3}Ni_{1/3}Mn_{1/3}O_2$ has a smaller change in unit-cell volume associated with lithium insertion reaction than those of $LiCoO_2$, $LiNiO_2$, and $LiMnO_2$. Compared with $LiCoO_2$ cathode material, $LiCo_{1/3}Ni_{1/3}Mn_{1/3}O_2$ cathode material has a series of excellent properties. Related researchers are expected to exceed $LiCoO_2$ cathode materials in terms of its use value [6–8]. However, $LiNi_{1/3}Co_{1/3}Mn_{1/3}O_2$ still has some disadvantages; the most prominent defect is the initial charge and discharge [9–11]. The initial charge–discharge irreversible capacity difference of $LiNi_{1/3}Co_{1/3}Mn_{1/3}O_2$ is 40–100 $mAh{\cdot}g^{-1}$ [12]. This phenomenon can explained by the following reasons: (1) some transition metals are dissolved in the organic electrolyte during the charge–discharge reaction; therefore, the active material is reduced that is why the capacity is reduced and (2) after the first cycle, the form of O changed to O^{2-}; precipitation results in rearrangement of anionic cation and reduction of active substances [13, 14], which lead to Li^+ cannot be re-embedded and the capacity will be reduced [15].

Moreover, low conductivity, structural stability, and low vibration density are still the technical bottlenecks of $LiNi_{1/3}Co_{1/3}Mn_{1/3}O_2$ cathode material. Elemental doping and surface modification [16, 17] are effective ways to improve its properties. Carbon, metal oxide, and metal element coating are commonly used for surface modification

✉ Zhongcai Shao
zcs18940221016@126.com

Lina Yv
1804396614@qq.com

Jing Wang
Wangjing@djtu.edu.cn

Xuetan Li
lixt@sylu.edu.cn

Lijing Dai
18840847557@162.com

[1] Liaoning Key Laboratory for Fabrication and Application of Superfine Inorganic Powders, Dalian Jiaotong University, Dalian, China

[2] Chemical Engineering, Shenyang Ligong University, Shenyang 116028, China

and doping of elements such as Zn [18], Al [19], Mg [20], Ti [21], Ti-F, Mg-F, and Mg-Cl [22].

Influences of doping metal oxide (TiO_2) on the structure and electrochemical properties of $LiNi_{1/3}Co_{1/3}Mn_{1/3}O_2$ cathode material are investigated. The morphology and structure of the samples were characterized by X-ray diffraction (XRD) and scanning electron microscopy (SEM). The electrochemical performances of $LiNi_{1/3}Co_{1/3}Mn_{1/3}O_2$ cathode material doped with metal oxide (TiO_2) are analyzed by galvanostatic testing, electrochemical impedance spectroscopy (EIS), and cyclic voltammetry (CV).

Experiment

According to the experimental scheme, $LiNi_{1/3}Co_{1/3-1/20}Mn_{1/3}Ti_{1/20}O_2$ composite was synthesized via co-precipitation method. Raw materials of nickel sulfate ($NiSO_4{\cdot}6H_2O$), cobalt sulfate ($CoSO_4{\cdot}7H_2O$), manganese sulfate ($MnSO_4{\cdot}4H_2O$), sodium hydroxide (NaOH), ammonium hydroxide ($NH_3{\cdot}H_2O$), and lithium hydroxide ($LiOH{\cdot}H_2O$) were employed; titanium dioxide (TiO_2) was adopted as dopant. All reagents used were of analytical grade. $NiSO_4{\cdot}6H_2O$ (0.033 mol), $CoSO_4{\cdot}7H_2O$ (0.028 mol), and $MnSO_4{\cdot}4H_2O$ (0.033 mol) were firstly dissolved in the deionized water (50 mL), and TiO_2 (0.005 mol) was added in the solution. Then NaOH (0.21 mol, 0.42 mol/L) solution used as precipitant was slowly added to the mixed solution, and $NH_3{\cdot}H_2O$ was used as a complexion agent to adjust the pH = 11 under stirring for 4 h. The precursor was obtained after filtered and dried. $LiOH{\cdot}H_2O$ (0.1 mol) was mixed, and then preheated at 500 °C (heating rate 5 °C/min) for 5 h and treated thermally at 850 °C (heating rate 5 °C/min) for 10 h to obtain $LiNi_{1/3}Co_{1/3-1/20}Mn_{1/3}Ti_{1/20}O_2$ composite.

For comparison purpose, $LiNi_{1/3}Co_{1/3}Mn_{1/3}O_2$ without doping Ti^{4+} was also prepared according to the procedure described above.

Cathode material, acetylene black, and polyvinylidene fluoride (PVDF) were weighed into a 25 × 25 mm weighing bottle according to the mass ratio of 80:10:10. Add appropriate amount of N-methylpyrrolidone, magnetically stir for 10 h, then uniformly spread the stirred slurry on aluminum foil with an area of about 40 × 80 mm, put it into a vacuum drying oven, and dry it at 80 °C for 10 h under vacuum. The dried active substance was tableted, punched, and loaded with a battery.

Characterizations and electrochemical measurement

The phase purity and crystal structure of the powder are identified by powder X-ray diffraction (XRD, D/MAX-2250 V, Rigaku) using Cu-Kα radiation ($\lambda = 0.15418$ nm) in the range of 10–80°, scanning speed is $12°{\cdot}min^{-1}$, operating voltage is 40 kV, and working current is 20 mA.

The morphology of the prepared TiO_2-doped $LiNi_{1/3}Co_{1/3}Mn_{1/3}O_2$ powder is observed by the JSM-6360-LV scanning electron microscope (SEM).

The electrochemical performance of $Li_{1/3}Co_{1/3-1/20}Mn_{1/3}Ti_{1/20}O_2$ is tested using a 2025 coin cell battery. The charge and discharge test is performed at a magnification of 0.1, 0.2, 0.5, and 1.0 C at room temperature.

Cyclic voltammetry (CV, 0.1 $mV{\cdot}s^{-1}$, 2.5–4.6 V) and electrochemical impedance spectroscopy (EIS, 2.5 V, 0.01–100 kHz) of the cells were measured on an electrochemical workstation (CHI660E, Shanghai Chenhua, China). All measurements are taken at room temperature.

Results and discussion

The XRD spectrum of $LiNi_{1/3}Co_{1/3}Mn_{1/3}O_2$ and $LiNi_{1/3}Co_{1/3-1/20}Mn_{1/3}Ti_{1/20}O_2$ cathode material is shown in Fig. 1. Compared with the standard spectrum, the crystal structure of $LiNi_{1/3}Co_{1/3}Mn_{1/3}O_2$ and $LiNi_{1/3}Co_{1/3-1/20}Mn_{1/3}Ti_{1/20}O_2$ was characterized by α-$NaFeO_2$ layered structure and belong to the $NaFeO_2$-type layered structure [23]. There was no impurity which was consistent with TiO_2 in the XRD pattern of $LiNi_{1/3}Co_{1/3-1/20}Mn_{1/3}Ti_{1/20}O_2$. Results manifested that a low amount of Ti-doped could be successfully doped into $LiNi_{1/3}Co_{1/3}Mn_{1/3}O_2$ without affecting the structure.

Furthermore, $I(003)/I(104)$ reflects the layered structure of the sample crystal [24]; the ratio more than 1.2 is beneficial to improve the electrochemical performance of the material. As shown in Table 1, the ratios of $I(003)/I(104)$ for $LiNi_{1/3}Co_{1/3-1/20}Mn_{1/3}Ti_{1/20}O_2$ and $LiNi_{1/3}Co_{1/3}Mn_{1/3}O_2$ were 1.512 and 1.425, respectively. The ratio of $I(003)/I(104)$

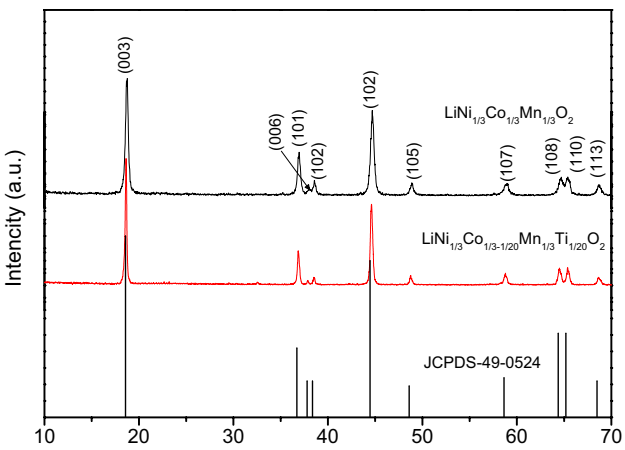

Fig. 1 XRD spectra of $LiNi_{1/3}Co_{1/3}Mn_{1/3}O_2$ and $LiNi_{1/3}Co_{1/3-1/20}Mn_{1/3}Ti_{1/20}O_2$

Table 1 XRD spectral analysis of $LiNi_{1/3}Co_{1/3-1/20}Mn_{1/3}Ti_{1/20}O_2$

Coating	*a*/nm	*c*/nm	*c*/*a*	$I_{(003)}/I_{(104)}$
$LiNi_{1/3}Co_{1/3}Mn_{1/3}O_2$	0.2866	1.4255	4.9738	1.437
$LiNi_{1/3}Co_{1/3-1/20}Mn_{1/3}Ti_{1/20}O_2$	0.2865	1.4258	4.9766	1.514

a, *c* represent unit cell parameter value, *c*/*a* represents the unit cell parameters ratio, *I*(003)/*I*(104) is peak strength ratio of *I*(003) and *I*(104)

increased after doping Ti-ion, which indicated that the cation mixing degree of the composite structure was reduced; the cations were arranged in order. Moreover, doping a small amount of Ti-ion, Ni-ion can be inhibited from occupying the lithium in the lithium layer, which was beneficial to improve the electrochemical performance of the material.

Figure 2 shows SEM of $LiNi_{1/3}Co_{1/3}Mn_{1/3}O_2$ and $LiNi_{1/3}Co_{1/3-1/20}Mn_{1/3}Ti_{1/20}O_2$. We noticed that the particles of $LiNi_{1/3}Co_{1/3}Mn_{1/3}O_2$ were well-distributed, and the size of particles was estimated to be 1–2 μm. However, compared with $LiNi_{1/3}Co_{1/3}Mn_{1/3}O_2$, $LiNi_{1/3}Co_{1/3-1/20}Mn_{1/3}Ti_{1/20}O_2$ had smaller particle size which was estimated to be 0.5–1.5 μm. The reason is that Ti^{4+} occupied the position of $(Ni_{1/3}Co_{1/3}Mn_{1/3})^{3+}$; the charge of Ti^{4+} was much larger than that of $(Ni_{1/3}Co_{1/3}Mn_{1/3})^{3+}$, causing lattice distortion, which reduced the surface energy of $LiNi_{1/3}Co_{1/3}Mn_{1/3}O_2$ crystal and reduced the driving force of crystal growth, thereby hindering the increase in crystal size during the synthesis of $LiNi_{1/3}Co_{1/3-1/20}Mn_{1/3}Ti_{1/20}O_2$ material. Smaller particle size was beneficial to short the diffusion distance of Li-ion and increase the diffusion rate of Li-ion.

Figure 3 shows EDS maps of $LiNi_{1/3}Co_{1/3-1/20}Mn_{1/3}Ti_{1/20}O_2$. The EDS maps revealed the presence of O element (pink), Mn element (light blue), Co element (purple), Ni element (dark blue), and Ti element (green), respectively. Moreover, it can be seen that not only nickel, cobalt, and manganese elements were uniformly distributed on the particle surface, but also titanium element was uniformly distributed. The result indicated that Ti successfully doped into $LiNi_{1/3}Co_{1/3}Mn_{1/3}O_2$ and homogeneously distributed [25].

In order to test the charging and discharging properties of the materials, the materials were assembled into button batteries for testing. Figure 4 shows the initial charge and discharge curves of and $LiNi_{1/3}Co_{1/3-1/20}Mn_{1/3}Ti_{1/20}O_2$ at a rate of 0.1 C. It can be seen that $LiNi_{1/3}Co_{1/3-1/20}Mn_{1/3}Ti_{1/20}O_2$ had an irreversible potential platform at 4.25 V during charging. The platform belonged to a small reversible delithiation deoxidation (Li_2O) process. The first charge–discharge specific capacities of $LiNi_{1/3}Co_{1/3-1/20}Mn_{1/3}Ti_{1/20}O_2$ at 0.1 C-rate were 173.3 and 170.3 $mAh{\cdot}g^{-1}$, while the first charge–discharge specific capacities of $LiNi_{1/3}Co_{1/3}Mn_{1/3}O_2$ were 158.8 and 155.1 $mAh{\cdot}g^{-1}$. The coulomb efficiencies were 98.2% and 96%, respectively. Compared with the initial charge–discharge performance of $LiNi_{1/3}Co_{1/3}Mn_{1/3}O_2$, the initial charge–discharge specific capacity of $LiNi_{1/3}Co_{1/3-1/20}Mn_{1/3}Ti_{1/20}O_2$ was much larger than those of $LiNi_{1/3}Co_{1/3}Mn_{1/3}O_2$. This is due to the small agglomeration of material particles, uniform particle size, and tight combination. The large surface area is beneficial to the deintercalation of lithium ions on the surface of the electrode and improves the charge and discharge performance of the material.

Figure 5 shows the discharge cycle of $LiNi_{1/3}Co_{1/3}Mn_{1/3}O_2$ and $LiNi_{1/3}Co_{1/3-1/20}Mn_{1/3}Ti_{1/20}O_2$ at 0.1 C-rate. After 100 cycles, the discharge capacity of $LiNi_{1/3}Co_{1/3-1/20}Mn_{1/3}Ti_{1/20}O_2$ and $LiNi_{1/3}Co_{1/3}Mn_{1/3}O_2$ was 121.6 and 80.0 $mAh{\cdot}g^{-1}$ with the capacity retention rates of 71.4% and 54%, respectively. It can be seen that after 100 cycles of charge and discharge of $LiNi_{1/3}Co_{1/3-1/20}Mn_{1/3}Ti_{1/20}O_2$, the cycle performance was improved compared with $LiNi_{1/3}Co_{1/3}Mn_{1/3}O_2$, and the capacity retention rate was well. In the crystal structure of $LiNi_{1/3}Co_{1/3-1/20}Mn_{1/3}Ti_{1/20}O_2$, Ti^{4+} is in a constant valence

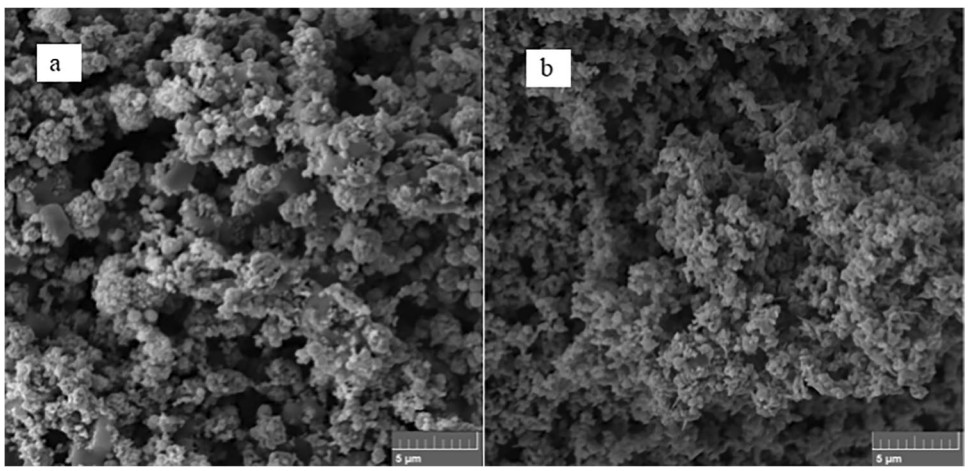

Fig. 2 SEM images of **a** $LiNi_{1/3}Co_{1/3}Mn_{1/3}O_2$ and **b** $LiNi_{1/3}Co_{1/3-1/20}Mn_{1/3}Ti_{1/20}O_2$, respectively

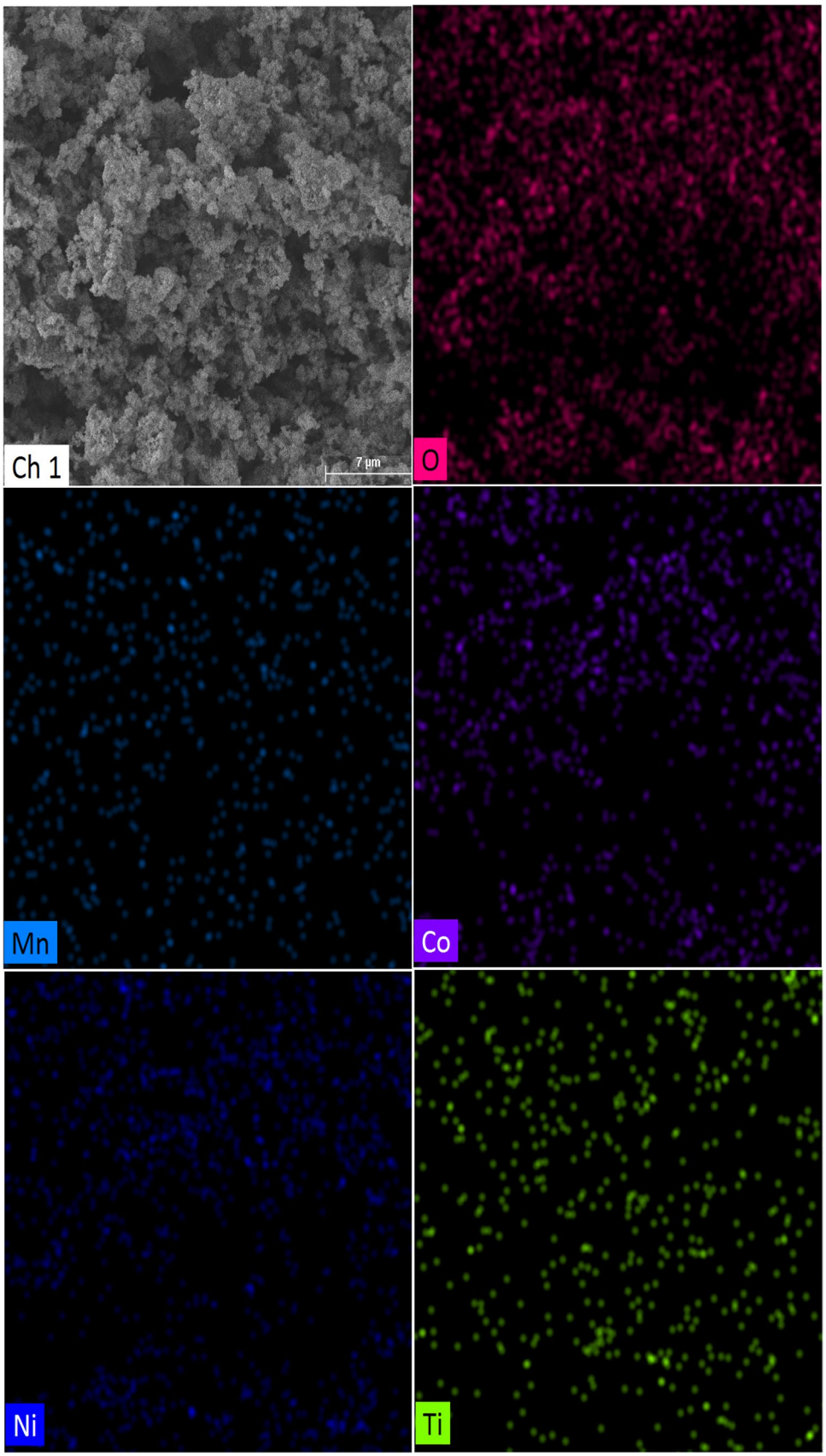

Fig. 3 EDS of $LiNi_{1/3}Co_{1/3-1/20}Mn_{1/3}Ti_{1/20}O_2$

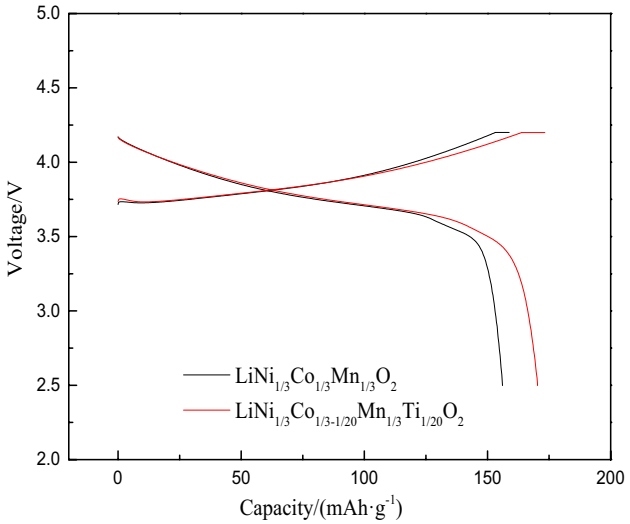

Fig. 4 The initial charge–discharge curves of $LiNi_{1/3}Co_{1/3}Mn_{1/3}O_2$ and $LiNi_{1/3}Co_{1/3-1/20}Mn_{1/3}Ti_{1/20}O_2$ at a rate of 0.1 C

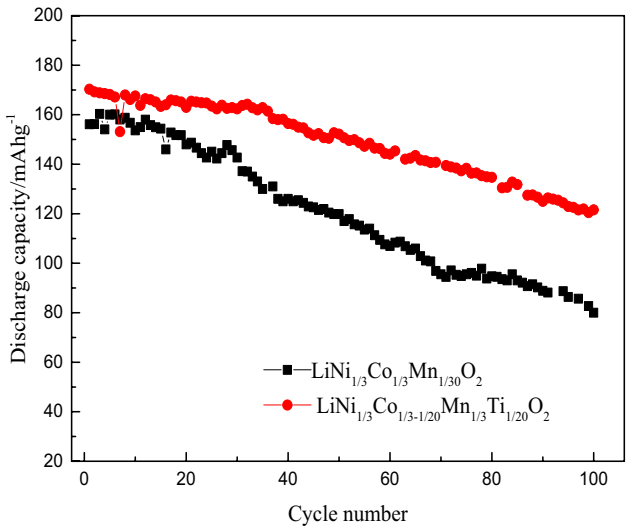

Fig. 5 Cycling performance of $LiNi_{1/3}Co_{1/3}Mn_{1/3}O_2$ and $LiNi_{1/3}Co_{1/3-1/20}Mn_{1/3}Ti_{1/20}O_2$ at a rate of 0.1 C

state, does not participate in the electrochemical reaction, and plays as a "skeleton" support role, ensuring the smooth extraction and embedding of lithium ions in the active material lattice framework. Effectively avoid material changes during charging and discharging, so the cycle performance of the material is significantly improved.

To further explore the effect of Ti-doped on the material, we tested the rate performance of the sample. Figure 5 shows the discharge curves of $LiNi_{1/3}Co_{1/3-1/20}Mn_{1/3}Ti_{1/20}O_2$ and $LiNi_{1/3}Co_{1/3}Mn_{1/3}O_2$ at different rates from 0.2 to 5.0 C. The discharge specific capacities of $LiNi_{1/3}Co_{1/3-1/20}Mn_{1/3}Ti_{1/20}O_2$ at rates of 0.2, 0.5, 1, 2, and 5 C were 166.1, 150.5, 138.3, 120.5, and 92.8 $mAh{\cdot}g^{-1}$, respectively. The discharge specific capacities of $LiNi_{1/3}Co_{1/3}Mn_{1/3}O_2$ at different discharge rates were 137.4, 112.7, 109.4, 88.8, and 65.2 $mAh{\cdot}g^{-1}$. When the charge–discharge rate increases, the charge–discharge specific capacity of the material gradually decreases because the charge–discharge cycle is a process of lithium-ion insertion and removal. As the electrode reaction proceeds, lithium-ion cannot migrate from the positive or negative direction, thereby increasing the charging voltage, lowering the discharge voltage, and lowering the discharge capacity. After doping Ti^{4+}, the volume of the battery increases, which expands the diffusion path of lithium ions, promotes the diffusion of lithium ions, and thereby increases the discharge capacity of the material (Fig. 6).

Figure 7 shows the cycle performance of the cathode material at different rates. It can be seen that the capacity decay after doping with Ti is relatively low, and the capacity retention rates are 56.3% and 44.1%, respectively. The doping of Ti can suppress the collapse of the material structure caused by the change of Ni ion radius during charging and discharging to a certain extent. Lithium ions have a higher extraction and insertion rate, and the polarization of the electrode is reduced, thereby stabilizing the electrochemistry of the cathode material.

Figure 8 shows EIS of $LiNi_{1/3}Co_{1/3}Mn_{1/3}O_2$ and $LiNi_{1/3}Co_{1/3-1/20}Mn_{1/3}Ti_{1/20}O_2$. The EIS was composed of three parts, the high-frequency region, the low-frequency region, and the high-frequency region and the impedance real axis. A small intercept composition, wherein the semicircle of the first half represented a high-frequency region, indicating the retardation of the charge transfer speed during the movement of electrons inside the battery, that is, the speed of the electron movement was greater than the impedance caused by the formation of the electric double layer by the electrode reaction speed. A straight line represents the low-frequency region, indicating the diffusion impedance, and the diffusion process of Li^+ between the electrode surface and the electrolyte; the intersection of the high-frequency region curve and the real axis of the impedance reflects the inherent impedance of the battery, including the electrolyte and the diaphragm. The intersection of the high frequency curve with the impedance real axis reflects the inherent impedance of the battery, including electrolytes and the sum of the impedances other than those of the electrodes [26].

It is the equivalent circuit diagram obtained by simulation with Zview software. The resistance caused by the diffusion of charge in the positive electrode material and the resistance of the electric double layer formed by the charge moving too fast (R_s), impedance caused by the transfer of Li^+ at the interface between the cathode material and the electrolyte (R_{ct}), and the constant phase angle element. And Warburg impedance (W_S). The charge transfer impedances

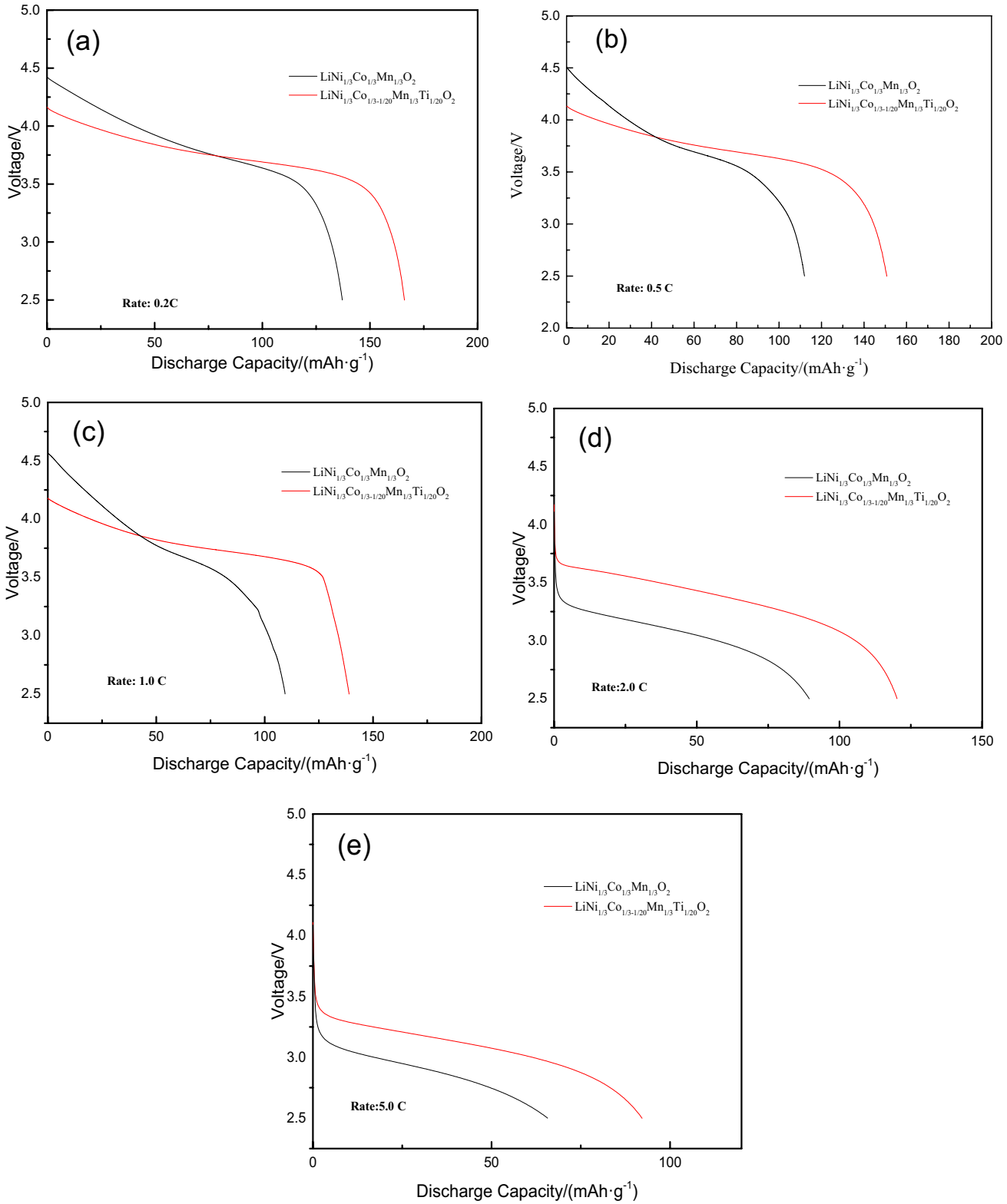

Fig. 6 The discharge curves of $LiNi_{1/3}Co_{1/3}Mn_{1/3}O_2$ and $LiNi_{1/3}Co_{1/3-1/20}Mn_{1/3}Ti_{1/20}O_2$ at different rates of 0.2, 0.5, and 1.0 C (**a** 0.2 C, **b** 0.5 C, **c** 1.0 C, **d** 2.0 C, **e** 5.0 C)

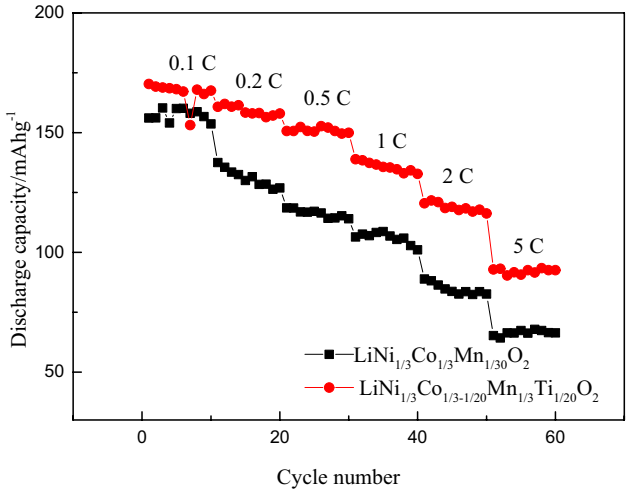

Fig. 7 Cyclic performance diagram at different magnifications

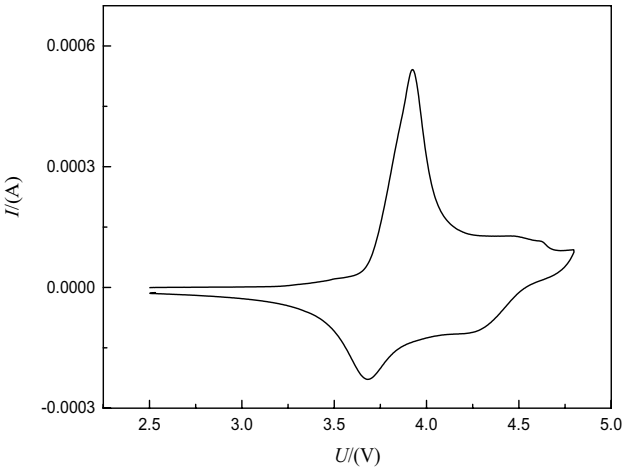

Fig. 9 Cyclic voltammetry curve of $LiNi_{1/3}Co_{1/3-1/20}Mn_{1/3}Ti_{1/20}O_2$

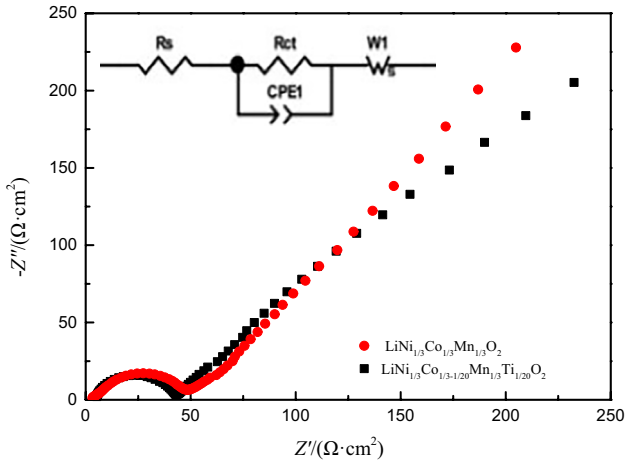

Fig. 8 EIS plots of $LiNi_{1/3}Co_{1/3}Mn_{1/3}O_2$ and $LiNi_{1/3}Co_{1/3-1/20}Mn_{1/3}Ti_{1/20}O_2$

of Ti doped and Ti undoped are 450 and 480 Ω, respectively. It can be seen from Fig. 8 that $LiNi_{1/3}Co_{1/3-1/20}Mn_{1/3}Ti_{1/20}O_2$ material had a lower impedance than $LiNi_{1/3}Co_{1/3}Mn_{1/3}O_2$ material, which indicates that $LiNi_{1/3}Co_{1/3-1/20}Mn_{1/3}Ti_{1/20}O_2$ displayed a smaller charge transfer resistance. The smaller charge transfer resistance was regarded to be favorable for overcoming the restriction of kinetics in the charge/discharge process, which could enhance the diffusion of Li^+.

Figure 9 shows the cyclic voltammetry of $LiNi_{1/3}Co_{1/3-1/20}Mn_{1/3}Ti_{1/20}O_2$ material. It can be seen that there was a pair of redox peaks in the curve, wherein the oxidation peak represents the removal process of Li^+ and the reduction peak represents the removal process. It is clear that the symmetry of the redox peak is better, which proves that the electroactive material of the material synthesized under optimized conditions is reversible [27, 28]. As can be seen from Fig. 8, the difference between the two peaks in the cyclic voltammetry of $LiNi_{1/3}Co_{1/3-1/20}Mn_{1/3}Ti_{1/20}O_2$ material was small, indicating that the polarization of the electrode was very small. This is because when the current passes, the reaction speed of the electrode lags behind the reaction speed of the electron, which causes charge accumulation and polarization at the interface, resulting in an electrochemical polarization potential. Doping Ti^{4+} makes it easier to remove lithium ions during charging and discharging, and charge transfer is faster and electrochemical performance is better.

Conclusion

In this paper, $LiNi_{1/3}Co_{1/3-1/20}Mn_{1/3}Ti_{1/20}O_2$ composites were obtained by co-deposition method. The effects of Ti-doped on the structure, morphology, and electrochemical properties of samples were studied. Results indicated that a low amount of Ti-doping could be successfully doped into $LiNi_{1/3}Co_{1/3}Mn_{1/3}O_2$ without affecting the structure. $LiNi_{1/3}Co_{1/3-1/20}Mn_{1/3}Ti_{1/20}O_2$ had small particle size which was estimated to be 0.5–1.5 μm. Moreover, $LiNi_{1/3}Co_{1/3-1/20}Mn_{1/3}Ti_{1/20}O_2$ delivered a high initial discharge capacity of 170.3 mAh g^{-1} with a coulombic efficiency of 98% at a rate of 0.1 C. In summary, the obtained $LiNi_{1/3}Co_{1/3}Mn_{1/3}O_2$ sample with doping Ti-ion showed a well-crystallized structure and excellent electrochemical performance.

Declarations

Conflict of interest The authors declare no competing interests.

References

1. Lu X, Li ZX, Wang ZX, Guo H, Yan G, Yin X (2014) A modified co-precipitation process to coat $LiNi_{1/3}Co_{1/3}Mn_{1/3}O_2$ onto $LiNi_{0.8}Co_{0.1}Mn_{0.1}O_2$ for improving the electrochemical performance. Appl Surf Sci 297(1):182–187
2. Koyama Y, Tanaka I, Adachi H, Makimura Y, Ohzuku T (2003) Crystal and electronic structures of superstructural $Li_{1-x}[Ni_{1/3}Co_{1/3}Mn_{1/3}]O_2(0\leq x \leq 1)$. J Power Sources 119–121(1):644–648
3. Chen H, Hu Q, Huang Z, He Z, Wang Z, Guo H, Li X (2016) Synthesis and electrochemical study of Zr-doped $[Li_{0.2}Mn_{0.54}Ni_{0.13}Co_{0.13}]$ as cathode material for Li-ion battery. Ceram Int 42(1):263–269
4. Yabuuchi N, Ohzuku T (2003) Novel lithium insertion material of $LiNi_{1/3}Co_{1/3}Mn_{1/3}O_2$for advanced lithium-ion batteries. J Power Sources 119(9):171–174
5. Deng S, Chen Y, Koliopoulos G, Papangelakis VG, Li Y (2020) Thermodynamic and experimental analysis of Ni-Co-Mn carbonate precursor synthesis for Li-rich cathode materials. Ionics 437(26):2747–2755
6. Zhu L, Bao C, Xie L, Yang X, Cao X (2020) Review of synthesis and structural optimization of $LiNi_{1/3}Co_{1/3}Mn_{1/3}O_2$ cathode materials for lithium-ion batteries applications. J Alloys Compd 831(7):154864
7. Li H, Hu S, Zhang J, Qin H, Chao M (2020) Electrochemical performance of Sn-doped cobalt-free $Li_{1.15}Ni_{0.27}Mn_{0.58-x}Sn_xO_2$ cathode material for Li-ion batteries. Ionics 253(26):3785–3794
8. Wu Y, Manthiram A (2009) Effect of surface modifications on the layered solid solution cathodes $(1-z)Li[Li_{1/3}Mn_{2/3}]O_{2-z}Li[Mn_{0.5-y}Ni_{0.5-y}Co_{2y}]O_2$. Solid State Ionics 180(1):50–56
9. Nie M, Xia YF, Wang ZB (2015) Effects of precursor particle size on the performance of $LiNi_{0.5}Co_{0.2}Mn_{0.3}O_2$ cathode material. Ceram Int 141(10):15185–15192
10. Zhang Z, Zhu S, Huang J (2016) Acacia gum-assisted coprecipitating synthesis of $LiNi_{0.5}Co_{0.2}Mn_{0.3}O_2$, cathode material for lithium ion batteries. Ionics 22(5):621–627
11. Yan G, Li X, Wang Z (2015) Effects of 1-propylphosphonic acid cyclic anhydride as an electrolyte additive on the high voltage cycling performance of graphite/$LiNi_{0.5}Co_{0.2}Mn_{0.3}O_2$ battery. Electrochim Acta 166(1):190–196
12. Xiao ZW, Zhang YJ, Wang YF (2015) Synthesis of high-capacity $LiNi_{0.8}Co_{0.1}Mn_{0.1}O_2$ cathode by transition metal acetates. T Nonferr Metal Soc 25(5):1568–1574
13. Li Y, Liu KY, Lv MY, Wei L, Zhong JJ (2014) Synthesis characterization and electrochemical performance of AlF_3 coated $Li_{1.2}(Mn_{0.54}Ni_{0.16}Co_{0.08})O_2$ as cathode for Li-ion battery. T Nonferr Metal Soc 24(11):3534–3540
14. Chang ZR, Lv HJ, Tang HW, Li HJ, Yuan XZ, Wang H (2009) Synthesis and characterization of high-density $LiFePO_4$/C composites as cathode materials for lithium-ion batteries. Electrochim Acta 54(20):4595–4599
15. Cho YD, Fey GTK, Kao HM (2009) The effect of carbon coating thickness on the capacity of $LiFePO_4$/C composite cathodes. J Power Sources 189(1):256–262
16. Patey TJ, Büchel R, Ng SH, Krumeich F, Patshinis SE, Novák, (2009) Flame co-synthesis of $LiMn_2O_4$ and carbon nanocomposites for high power batteries. J Power Sources 189(1):149–154
17. Lin F, Markus IM, Nordlund D, Weng TC, Asta MD (2014) Surface reconstruction and chemical evolution of stoichiometric layered cathode materials for lithium-ion batteries. Nat Commun 27(5):23–31
18. Bak SM, Hu E, Zhou Y (2014) Structural changes and thermal stability of charged $LiNi_xMn_yCo_zO_2$ cathode materials studied by combined in situ time-resolved XRD and mass spectroscopy. Appl Mater Inter 24(6):22594–22601
19. Li X, Qiu K, Gao Y (2015) High potential performance of cerium-doped $LiNi_{0.5}Co_{0.2}Mn_{0.3}O_2$ cathode material for Li-ion battery. J Mater Sci 50(7):2914–2920
20. Mao X, Liang X, Liu J, Li D (2018) Effect of Zn doping on the structure and electrochemical performance of $LiNi_{1/3}Co_{1/3}Mn_{1/3}O_2$. Rare Metal Mat Eng 44(3):743–747
21. Tarutin AP, Lyazaeva JG, Farlenkow AS, Vyikov AI, Medvedev DA (2019) Cu-substituted $La_2NiO^{4+}\delta$ as oxygen electrodes for protonic ceramic electrochemical cells. J Mater Sci 45(13):16105–16112
22. Hu G, Zhang MF, Liang LW, Peng ZD, Du K, Cao YB (2016) Mg-Al-B co-substitution $LiNi_{0.5}Co_{0.2}Mn_{0.3}O_2$ cathode materials with improved cycling performance for lithium-ion battery under high cutoff voltage. Electrochim Acta 190(1):264–275
23. Kim J, Park YU, Seo DH (2011) Mg and Fe Co-doped Mn based olivine cathode material for high power capability. J Electrochem Soc 158(3):250–254
24. Tang Y, Han X, Zhang W, He Y (2020) La doping and coating enabled by one-step method for high performance $Li_{1.2}Mn_{0.54}Ni_{0.13}Co_{0.13}O_2$ Li-rich cathode. Ionics 26(383):3737–3747
25. Zhang Y, Mei HX, Yang J, Wang SW, Gao KZ (2020) New $NiMoO_4$/$CoMoO_4$composite electrodes for enhanced performance supercapacitors. Ionics 304(26):3579–3590
26. Li YJ, Ren M, Han Q (2014) Structural changes and electrochemical properties of $LiNi_{0.5}Co_{0.2}Mn_{0.3}O_2$ cathode materials for lithium-ion batteries during heat treatment. T Nonferr Metal Soc 24(7):1785–1791
27. Wu Z, Ji S, Zheng J (2015) Prelithiation activates $LiNi_{0.5}Mn_{0.3}Co_{0.2}O_2$ for high capacity and excellent cycling stability. Nano Lett 15(8):5590–5596
28. Li L, Chen Z, Zhang Q (2014) A hydrolysis-hydrothermal route for the synthesis of ultrathin $LiAlO_2$-inlaid $LiNi_{0.5}Co_{0.2}Mn_{0.3}O_2$ as a high-performance cathode material for lithium ion batteries. J Mater Chem A 3(2):894–904